ARTICLE

A novel quartz-crystal microbalance humidity sensor based on solution-processible indium oxide quantum dots

Received 00th January 20xx,
Accepted 00th January 20xx

DOI: 10.1039/x0xx00000x

Hao Kan[a,b#], Min Li[c], Hui Li[a], Chong Li[a], Jian Zhou[d], Chen Fu[a], Jingting Luo[a*], Yongqing Fu[e]

Large surface area, like quantum confinement effect also caused by particular nano level size of quantum dots (QDs), brings fantastic possibility for humidity sensing. High concentration of surface adsorption site initiate response increasing. Porosity between QDs stacking up fast water vapor penetration and flowing away. Here, a quartz-crystal microbalance (QCM) humidity sensor was prepared using the indium oxide (In_2O_3) QDs, synthesized via solvothermal method. After In_2O_3 QDs directly spin-coating onto the QCM, an annealing process taken place to remove organic long chains and expose more moisture adsorption sites on the surface of the QDs. The annealed QCM humidity sensor exhibited high sensitivity (56.3 Hz/%RH at 86.3% RH), with a fast response/recovery time (14 s/16 s). Long carbon chains break down and hydrogen-bonded hydroxyl groups chemisorpted to the QDs. Chemical reaction was reduced by these chemisorpted hydrogen-bonded hydroxyl groups. Mass changing was mostly caused by fast multilayer physiorption. So the transducer can effectively and precisely monitor the moisture of person's breathing. In_2O_3 QDs modified QCM sensors demonstrating its promising humidity sensing applications in daily life.

Introduction

Humidity sensors have been widely used in the fields of chemistry, electronics, food storage, mining, meteorology, agriculture and medicine, etc..[1-4] Accurate and real-time monitoring of humidity is also critical for human safety and social activities. Therefore, it is critically required to develop a high-performance, repeatable and low-cost humidity sensor. So far, various of sensing technologies have been developed for humidity sensors, including resistance, optical, magnetic, capacitance acoustic and thermal, etc..[5-9] Among these, quartz crystal microbalance (QCM) is one of the most promising and key technology due to their merits such as low power consumption, easy operation, low cost, good sensitivity and extremely trace mass detection. By monitoring the shifts of the resonance frequency in real time, the mass change caused by water molecules can be precisely detected using the Sauerbrey equation.[10] Therefore, QCM sensors have been extensively researched as humidity sensors by more and more researchers.[11-15]

Based on the above advantages, various sensitive materials such as 0-dimensional (0D) QDs, 1-dimensional (1D) nanowires, graphene, reduced graphene oxide (RGO), black phosphorus and many types of polymers have been applied on the surface of QCM humidity sensors.[16-22] Obviously, these nanomaterials provide numerous reactive sites due to their larger specific surface areas, resulting in improved humidity sensing performance. Among them, 0D QDs exhibit wide-range potential applications in the field of humidity sensors due to their low cost, large specific surface areas and easy solution processes capabilities.[23-25] For example, Sun et al. prepared well-crystallized black phosphorus QDs from bulk black phosphorus using a kitchen blender, and the sensor using the black phosphorus QDs showed outstanding humidity sensing performance.[26] A flexible humidity sensor fabricated using graphene QDs was reported by Hossein et al., and the response of the transducer was quite high with good selectivity and flexibility.[27] Another QCM humidity sensor based on ZnO QDs sensitive film was reported by Sakly et al., and it exhibited high sensitivity, fast response/recovery speed and outstanding long-term stability.[28] Therefore, QDs with high specific surface area is a very promising type of humidity sensitive material.

Based on the discussion above, in the present work, we fabricated a QCM humidity sensor based on In_2O_3 QDs. The In_2O_3 QDs were spin-coated on the top of the electrodes of QCMs in the form of thin films, then the devices were annealed at 300°C in air for one hour to remove long chain carbons on the surface of the QDs. The humidity sensing performance of the QCM sensor was characterized at room temperature from 11.3% to 84.3% relative humidity (RH). It showed remarkable sensing characteristics, including high sensitivity (56.4 Hz/%RH), fast response/recovery (14 s/ 16 s) time, good stability and

[a.] *Shenzhen Key Laboratory of Advanced Thin Films and Applications, College of Physics and Optoelectronic Engineering, Shenzhen University, 518060, Shenzhen, China. Email: luojt@szu.edu.cn*
[b.] *Key Laboratory of Optoelectronic Devices and Systems of Ministry of Education and Guangdong Province, College of Optoelectronic Engineering, Shenzhen University, 518060, Shenzhen, China.*
[c.] *School of Electrical Engineering, Nanjing Institute of Industry Technology, 210023, Nanjing, China.*
[d.] *State Key Laboratory of Advanced Design and Manufacturing for Vehicle Body, College of Mechanical and Vehicle Engineering, Hunan University, Changsha 410082, China.*
[e.] *Faculty of Engineering and Environment, Northumbria University, Newcastle Upon Tyne, Newcastle NE1 8ST, UK.*

excellent selectivity for moisture. We believe this work provides a simple and easy way to fabricate a novel QCM humidity sensors based on In_2O_3 QDs.

Experimental section

In_2O_3 QDs synthesis and device preparation

The In_2O_3 QDs were synthesized via a modified method employing oleic acid (OA) and oleylamine (OLA) as the surfactants.[29] Briefly, 0.146g indium acetate, 12.5 mL OLA and 5 mL OA were mixed inside a three-necked flask. The mixtures were heated under vacuum at 90°C until indium acetate was completely dissolved. Then, the solution was kept under a nitrogen atmosphere and heated to 240°C for 30 min. Finally, In_2O_3 QDs were washed with ethanol and toluene, and eventually dispersed in toluene with a concentration of 20 mg/mL.

The QCM devices with a resonant frequency of 8 MHz were purchased from Wuhan Hi-Trusty Electronics Co., Ltd., China. It was consisted of an AT-cut quartz crystal (with size of 8 mm in diameter) and silver electrodes (with size of 5 mm in diameter) on both sides (Figure 1a). Before preparing In_2O_3 QDs film, all the QCM devices were washed with ethanol and deionized water, and then dried with nitrogen. The film coated QCM sensors were achieved by spin-coating method and post-annealing process (Figure 1b). Specifically, 20 µL In_2O_3 QDs solution was spin-coated onto the QCM device at 1200 rpm for 45 s. To remove organic long chains on the surface of In_2O_3 QDs, an annealing process in air at 300 °C for 1 h was carried out. This fabrication procedure of the QCM humidity sensor was shown in Figure 1b. In order to study the influences of the depositing amount of In_2O_3 QDs on sensing performance, three sensors with different deposition repeated cycles were prepared (2, 4, 6 times), which were marked as QCM-1, QCM-2 and QCM-3, respectively. The resonant frequency and the frequency after coating with the film were measured, and the mass of the In_2O_3 QDs deposited on the electrode of QCMs were calculated using the Sauerbrey equation.[10] All the detailed parameters of the samples are listed in Table 1.

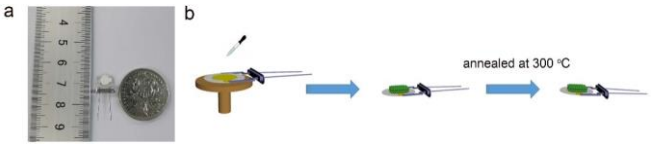

Figure 1. (a) The photograph of QCM device. (b) Fabrication procedure of the QCM humidity sensor based on In_2O_3 QDs.

Table 1. Preparation parameters of the fabricated samples

Samples	Fundamental frequency	Frequency shifts (Hz)	Load mass (ng)
QCM-1	7999890	-7266	9852
QCM-2	7999867	-14955	19794
QCM-3	7999799	-21004	28479

Sensing measurement

The schematic diagram of the experiment apparatus for the QCM humidity measurement is given in Figure 2. It was composed of QCM humidity sensor, humidity sources, computer and QCM-I (Microvacuum Ltd., Hungary). Saturated solutions of LiCl, $MgCl_2$, K_2CO_3, NaBr, NaCl and KCl were prepared which could provide different humidity environments in a conical flask with RH levels of 11.3%, 32.8%, 43.2%, 57.6%, 75.3% and 84.3% RH, respectively. The response time was defined as the time for the frequency change approaching 90% of the total frequency change, and the recovery time was defined as the time when the get back to 10% of the total frequency change. All the tests were performed at ambient temperature of 25°C.

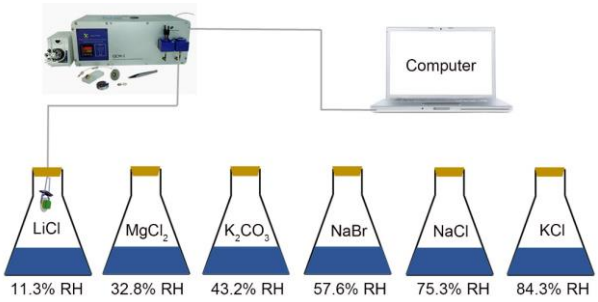

Figure 2. Schematic diagram of QCM humidity test system.

Characterization

X-ray diffraction (XRD) analysis of the QD films was performed using a diffractometer (MAXima XXRD-7000, Shimadzu, Japan) with Cu Kα radiation. The optical absorption spectra of the QDs were measured using a PerkinElmer Lambda 950 UV/vis/NIR spectrometer. Surface morphologies of the QDs samples were characterized using a scanning electron microscope (SEM, Zeiss Supra 55 microscope). High-resolution transmission electron microscopy (HR-TEM) was carried out using a JEOL-2100 microscope. The Fourier transform infrared (FTIR) spectroscopy were measurements by VERTEX 70 (Bruker, Germany).

Results and discussion

Figure 3a shows the crystallization characteristics of the In_2O_3 QDs. The XRD patterns of the synthesized In_2O_3 QDs are in good agreement with the standard diffraction results listed in the JCPDS card (NO. 65-3170), indicating the synthesized QDs have good crystallinity and no other impurities appear. Figure 3b shows a TEM image of In_2O_3 QDs. It was observed that the In_2O_3 QDs were uniformly dispersed and had an average diameter of 3.9 nm. This indicates that the diameter of the as-synthesized In_2O_3 QDs is less than twice of the Bohr exciton radius of the In_2O_3 (2.14 nm), confirming that the as-synthesized In_2O_3 has quantum size.[30,31] The transparent lattice fringes of atomic spacing associated with the (222) plane of the In_2O_3 phase can also be observed as shown in the inset of Figure 3b. This demonstrates that the In_2O_3 QDs have good crystallinity. Figure 3c shows the absorption spectrum of as-synthesized In_2O_3 QDs

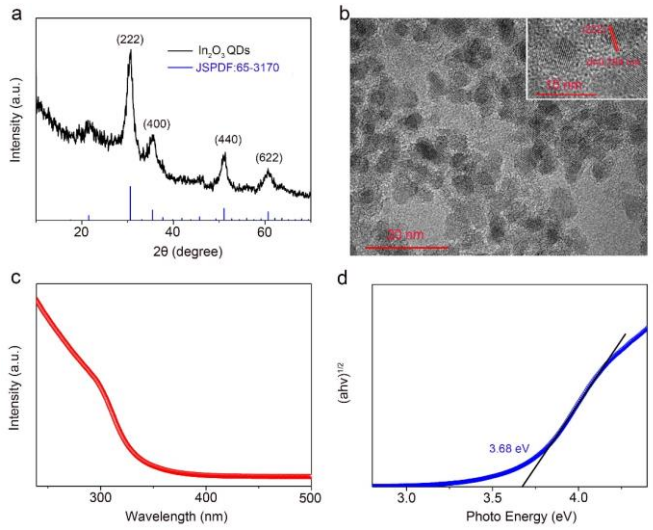

Figure 3. (a) XRD pattern of as-synthesized In_2O_3 QDs. (b) TEM image of the In_2O_3 QDs, the insets is HRTEM image of the In_2O_3 QDs (c) UV–vis absorption spectrum of the as-synthesized In_2O_3 QDs (d) The bandgap of the as-synthesized In_2O_3 QDs.

in hexane. The band gap of as-synthesized In_2O_3 QDs calculated by the Tauc model is about 3.68 eV (shown in the Figure 3d), which is larger than that of bulk In_2O_3 (2.93±0.15 eV). This result indicates that the as-synthesized In_2O_3 QDs have quantum confinement effect. As shown in Figure S1, the nitrogen adsorption and desorption isotherm cures of In2O3 QDs are investigated. The surface area of In2O3 QDs is calculated to be about 63.9 m2/g through the Brunauer Emmett Teller theory. As is known, high specific surface area can provide more active sites to promote the adsorption of water molecules, thus improving the humidity sensing.

The as-synthesized In_2O_3 QDs were capped with organic long-chain (OA and OLA), and these hydrophobic organic long-chains can inhibit water molecules to be adsorbed onto the surface of In_2O_3 QDs.[32,33] To remove the organic long chains, the In_2O_3 QDs films should be annealed at 300°C in air. In order to study the effect of annealing process on the QDs, we use FTIR to analyse the In_2O_3 QDs films before and after annealing, and the results are shown in Figure 4. Compared to the as-prepared In_2O_3 QDs film (red line), the characteristic absorption peaks of the aliphatic C-H stretching bands (2850-2920 cm-1) are

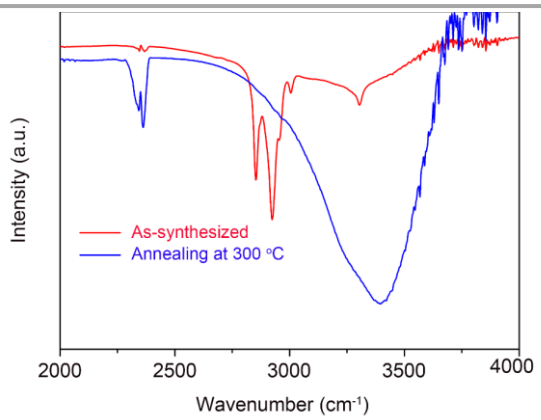

Figure 4. FTIR spectra of the untreated and annealed In_2O_3 QDs film.

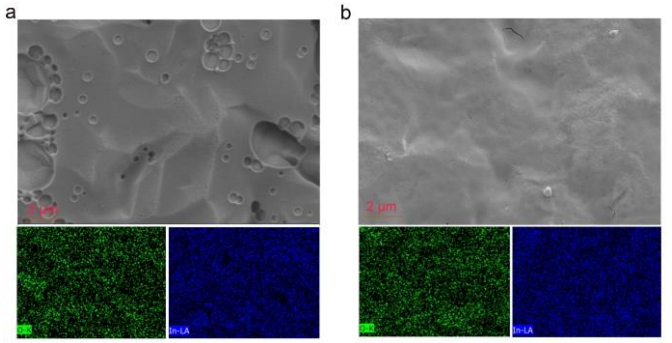

Figure 5. (a) The as-prepared In_2O_3 QDs film. (b) The In_2O_3 QDs film after annealed at 300°C for 1h.

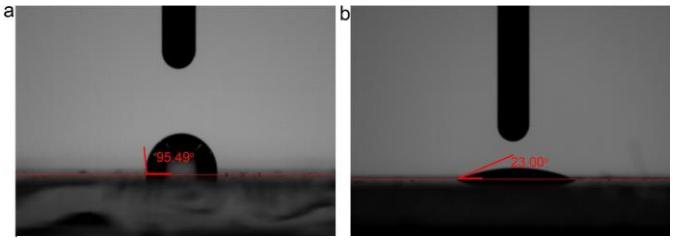

Figure 6. Contact angle measurement of (a) as-papered In_2O_3 QDs film, (b) In_2O_3 QDs film after annealing process.

disappeared after annealing process (blue line), indicating that most of the surface-capped OA and OLA ligands around the In_2O_3 QDs have been removed. As expected, after annealing process, a very strong characteristic peak at around 3445 cm^{-1} appeared (blue line), which is attributed to the hydrogen-bonded hydroxyl groups adsorbed on the In_2O_3 QDs. Results, indicate that the In_2O_3 QDs film has an outstanding hydrophilicity after annealing.

The SEM morphologies of the In_2O_3 QDs films before and after annealing were compared. Figure 5a is the SEM image of the as-deposited In_2O_3 QDs film with holes, which may be caused by the evaporation of solvent during the film formation process. After the film annealed at 300°C for 1h, the In_2O_3 QDs film becomes smoother but with some tiny cracks, which are generated owing to the densification with stress relaxation and the removal of organic long-chain ligands during the annealing process. This porous film is beneficial for the adsorption and diffusion of water molecules. The corresponding element mapping obtained from energy dispersive X-ray spectroscopy was shown in Figure 5. The elements of In and O were uniformly dispersed, which indicates that the QDs were uniformly deposited on the top of QCM electrode.

Figure 6 shows The wettability behaviours of In_2O_3 QDs film before and after annealing. The contact angle of the as-deposited QDs film is 95.49° (Figure 6a). This is due to the hydrophobicity of the surface-capped organic long chains. After annealing process, the contact angle of In_2O_3 QDs sensing film is as low as 23.00° (Figure 6b). This value verifies the excellent hydrophilicity of the In_2O_3 QDs sensing film. These results are consistent with FTIR spectrum. Also, the results of FTIR and contact angle suggest that the prepared QCM humidity sensor based on In_2O_3 QDs will have good humidity sensitivity.

The humidity sensitivity characteristic of the In_2O_3 QDs-based QCM sensor is quantified by changing the RH level in different saturated solution conical flask and measuring the changes of resonance frequency. Figure 7a shows the relationship between frequency shifts vs. RH for three sensors

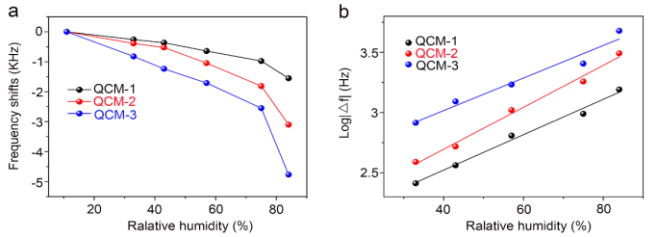

Figure 7. (a) The relationships between the frequency shifts of all the sensors. (b) the linear fitting curves of the Log |△f| versus humidity for all the sensors.

with test RH between 11.3% and 84.3%. As seen in the figure, the resonant frequency of all the sensors is decreased with the RH increasing. The frequency shifts are 1550 Hz, 3100 Hz and 4750 Hz for three QCM samples, respectively (with RH levels are changed from 11.3% to 84.3%). These indicate that the frequency shifts of the QCM humidity sensor based on In_2O_3 QDs is related to the deposited amount of In_2O_3 QDs. The QCM-3 sensor has the highest frequency offset (sensitivity). This indicates that greater amount of In_2O_3 QDs can adsorb more water molecules. As shown in Figure 7b, the frequency response of the three sensors exhibit very good log relationship with humidity, which is consistent with the results of other reported humidity sensors.[34,35] The regression coefficients R^2 of QCM-1, QCM-2 and QCM-3 sensors are 0.98411, 0.9899 and 0.97367, respectively.

QCM-3 sample with optimal humidity sensitivity were chosen for further testing. Figure 8a shows the dynamic frequency changes of the QCM-3 transducer. The sensor was tested twice with the RH levels changed from 11.3% RH to 32.8%RH, 43.2%RH, 57.6%RH, 75.3%RH and 84.3%RH. The frequency responses are not change significantly under the same humidity conditions, indicating that the humidity sensor has excellent RH measurement repeatability. The response / recovery time is another crucial parameter for evaluating humidity sensing performance. The response and recovery characteristic curves between RH levels of 11.3% and 75.3% are shown in Figure 8b. As can be seen, the response and recovery time of QCM-3 transducer are 14 s and 16 s, respectively, which indicates the sensor based on In_2O_3 QDs films have fast

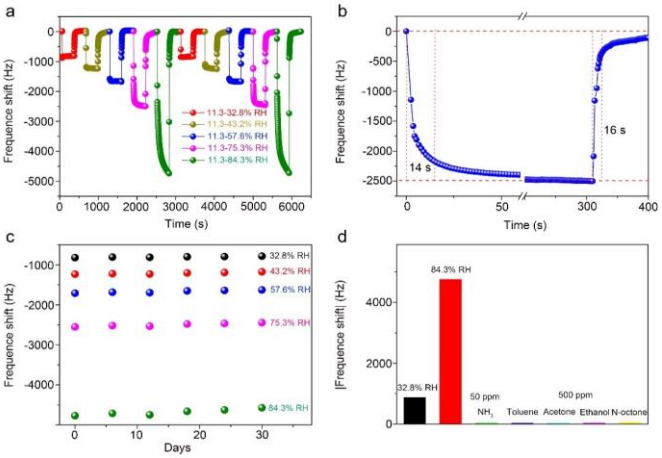

Figure 8. (a) The dynamic frequency shifts of the QCM-3 transducer. (b) The response and recovery curves between 11.3% and 75.3% conditions. (c) The long-term stability of the sensor. (d) The selectivity of QCM-3 at room temperature.

adsorption and desorption characteristics for water molecules. The long-term stability of the humidity sensor is very important for its practical application. Figure 8c shows the long-term stability of QCM humidity sensor based on In_2O_3 QDs. The frequency shifts of the sensor do not show apparent changes under different humidity conditions within 30 days. This result indicates that the sensor has a good long-term stability. The selectivity testing results of the QCM device are shown in Figure 8d. It demonstrated that the frequency shifts of the QCM sensor based on In_2O_3 QDs toward water molecules are much higher than those towards the commonly used target gases, including NH_3, ethanol, acetone, toluene, n-octane. Hence, the sensor has an excellent selectivity toward water molecules at room temperature. Finally, we summarized the reported humidity sensing performance of the QCM sensor in recent literature (Table 2). The results indicated that our sensor exhibits outstanding sensitivity and fast response and recovery times.

In order to demonstrate the application of QCM sensors based on In_2O_3 QDs for humidity detection, we further measure the human mouth breath via these sensors. As it is shown in Figure 9, breath from the mouth causes a sharp frequency decrease due to increase of the RH level suddenly. Hence, the

Table 2. The reported humidity sensing performance of the QCM sensor

Materials	RH Range (%)	Sensitivity	Response/Recovery time	Ref.
ZnO/GO	11-97	41.10Hz/%RH	9/5 s (@63.2%)	11
GQDs-chitosan	11-95	39.2 Hz/%RH	36/ 3 s (@95%)	36
SnO_2-SiO_2	11-96	9.4 Hz/%RH	14/ 16 s (@90%)	37
ZnO colloid spheres	11-95	77 Hz/%RH	167.7/ 8 s(@95%)	38
GO/PEI	11-97	27.3 Hz/%RH	53/18 s (@90%)	39
In_2O_3 QDs	11.3-84.3	56.3 Hz/%RH	14/16 s (@74.3%)	This work

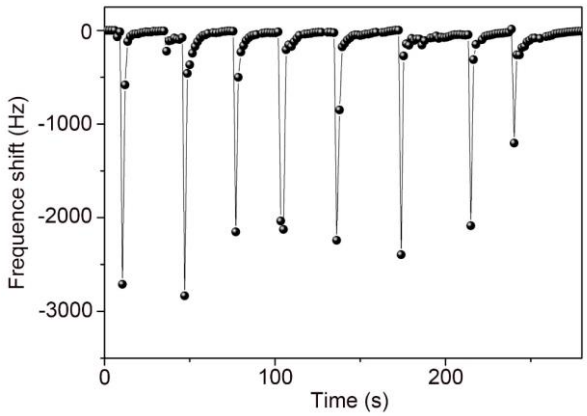

Figure 9. The frequency response of human mouth breath.

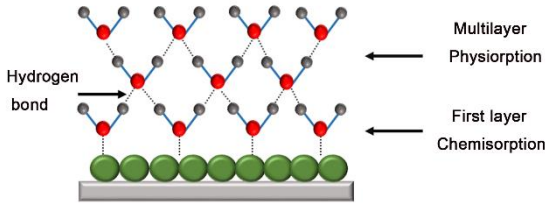

Figure 10. Schematic diagram of the humidity sensing mechanism of the In_2O_3 QDs QCM humidity sensor

QCM sensor can detect the human respiration. These results show that the In_2O_3 QDs QCM sensor possess outstanding sensitivity to humidity, which can be used for human survival.

The humidity sensing mechanism of the In_2O_3 QDs QCM humidity sensor depends on adsorption/desorption of water molecules (Figure 10). Here, In_2O_3 QDs have abundant surface oxygen vacancies and a large specific surface area, which play an important role in improving sensing performance. First, the chemical absorption of water molecules forms OH^- on the surface of In_2O_3 QDs. Second, more water molecules will be physically adsorbed on the hydroxyl groups through the van der Waals force. As the ambient humidity increases, more water molecules will be adsorbed on the surface of the sensitive film, and the resonant frequency will decrease due to the mass gain of the QCM surface. In contrast, as the environmental RH decreases, water molecules on the surface of the sensitive film are desorbed and released into the environment. Then, the mass loading effect is decreased and the resonant frequency is increased. More water molecules will need more time for relative balance absorb/desorb state, so the response/recovery time of the sensor will be longer at high humidity.

Conclusion

In summary, QCM humidity sensors were fabricated by employing In_2O_3 QDs that were synthesized using solventhermal method. The In_2O_3 QDs films were prepared by spin-coating due the well solution processing properties, then the films were annealed at 300°C in order to increase its surface hydrophilicity. This sensor has outstanding sensitivity and short response/recovery time for humidity detection. Meantime, the sensor has been used to monitor the breath of the mouth, showing its potential for fast humidity detection in practical application. Furthermore, we discussed the humidity sensing mechanisms of this sensor. This study provided a new QDs humidity sensing material and expanded the application of QDs in QCM humidity sensors.

Conflicts of interest

There are no conflicts to declare.

Acknowledgements

The authors gratefully acknowledge the support of the National Key Research and Development Program of China (Grant no. 2016YFB0402705), the China Postdoctoral Science Foundation (2019M653018). This work was also supported by National Natural Science Foundation of China (Grant no. 11704261, 51605485, 11575118), Shenzhen Science & Technology Project (Grant no. JCYJ20170817100658231, JCYJ20180507182439574 , JCYJ20180305124317872). Funding supports from UK Engineering Physics and Science Research Council (EPSRC EP/P018998/1).

References

1 S. Wei, D. D. Han, L. Guo, Y. Y. He, H. Ding, Y. L. Zhang and F. S. Xiao, *J. Colloid Interfaces Sci.*, 2014, **431**, 17–23.
2 E. Pál, V. Hornok, R. Kun, A. Oszkó, T. Seemann, I. Dékány and M. Busse, *J. Colloid Interfaces Sci*., 2012, **378**, 100–109.
3 P. Tian, X.Y Gao, G. Wen, L. S. Zhong, Z. Wang and Z. Guo, *J. Colloid Interfaces Sci.*, 2018, **532**, 517–526.
4 H. Kaden, F. Köniğer, M. Strømme, G.A. Niklasson and K. Emmerich, *J. Colloid Interfaces Sci.*, 2013, **411**, 16–26.
5 S. Kano, K. Kim and M. Fujii, *ACS Sens.*, 2017, **2**, 828-833.
6 B. B. Du, D. X. Yang, X. Y. She, Y. Yuan, D. Mao, Y. J. Jiang and F. F. Lu, *Sens. Actuators B: Chem.*, 2017, **251**, 180–184.
7 X. H. Le, X. Y. Wang, J. T. Pang, Y. J. Liu, B. Fang, Z. Xu, C. Gao, Y. Xu and J. Xie, Sens. Actuators B: Chem., 2018, 255, 2454–2461.
8 S. Choi, H. Y. Yu, J. Jang, M. Kim, S. Kim, H. S. Jeong and D. Kim, *Small*, 2018, **14**, 1703934.
9 B. Chethan, Y. T. Ravikiran, S. C. Vijayakumari, H. G. Rajprakash and S. Thomas, *Sens. Actuators B: Chem.*, 2018, **280**, 466–474.
10 Y. Dong and G. Feng, *Sens. Actuators B: Chem.*, 1995, **24**, 62–64.
11 Z. Yuan, H. L. Tai, X. H. Bao, C. H. Liu, Z. B. Ye and Y. D. Jiang, *Mater. Lett.*, 2016, **174**, 28–31.
12 J. b. Lin, N. B. Gao, J. M. Liu, Z. X Hu, H. Fang, X. H. Tan, H. Y. Li, H. Jiang, H. Liu, T. L. Shi and G. L. Liao, *J. Mater. Chem. A*, 2019, **7**, 9068.
13 X. L. Cha, F. F. Yu, Y. Fan, J. F. Chen, L. Y. Wang, Q. Xiang, Z. M. Duan and J. Q. Xu, *Sens. Actuators B: Chem.*, 2018, **263**, 436–444.
14 E. S. Muckley, L. Collins, A. V. Ievlev, X. Y. Ye, K. Kisslinger, B. G. Sumpter, N. V. Lavrik, C. Y Nam and I. N. Ivanov, *ACS Appl. Mater. Interfaces.*, 2018, **10**, 31745-31754.

15 N. B. Gao, H. Y Li, W. H. Zhang, Y. Z. Zhang, Y. Zeng, Z. X. Hu, J. Y. Liu, J. J. Jiang, L. Miao, F. Yi, and H. Liu, S*ens. Actuators B: Chem.*, 2019, **293**, 129–135.
16 M. A. Mahjoub, G. Monier, C.R. Goumet, F. Reveret, M. Echabaane, D. Chaudanson, M. Petit, L. Bideux, B. Gruzza, J. Phys. Chem. C, 2016, 120, 11652-11662.
17 Z. Q. Wei, Z. K. Zhou, Q. Y. Li, J. C. Xue, A. D. Falco, Z. J. Yang, J. H. Zhou and X. H. Wang, *Small*, 2017, **13**, 1700109.
18 C. Melios, A. Centeno, A. Zurutuza, V. Panchal, C. E. Giusca, S. Spencer, S. P. Silva and O. Kazakova, *Carbon*, 2016, **103**, 273-280.
19 L. T. Duy, T. Q. Trung, V. Q. Dang, B. Hwang, S. Siddiqui, I. Y. Son, S. K. Yoon, D. J. Chung and N. E. Lee, *Adv. Funct. Mater.*, 2016, **26**, 4329–4338.
20 P. Yasaei, A. Behranginia, T. Foroozan, M. Asadi, K. Kim, F.K. Araghi and A.S. Khojin, *ACS Nano*, 2015, **9**, 9898–9905.
21 M. B. Erande, M. S. Pawar and D. J. Late, *ACS Appl. Mater. Interfaces*, 2016, **8**, 11548-11556.
22 S. H. Wu, G. H. Wang, Z. Xue, F. Ge, G. B. Zhang, H. B. Lu and L. Z. Qiu, *ACS Appl. Mater. Interfaces*, 2017, **9**, 14974-14982.
23 T. Alizadeh and M. Shokri, *Sens. Actuators B: Chem.*, 2016, **222**, 728–734.
24 Z. Lu, Y. Q. Gong, X. J. Li and Y. Zhang, *Appl. Surf. Sci.*, 2017, **399**, 330–336.
25 S. Yadav, P. Chaudhary, K. N. Uttam, A. Varma, M. Vashistha and B. C. Yadav, *Nanotechnology*, 2019, **30**, 295501.
26 C. Y. Zhu, F. Xu, L. Zhang, M. L. Li, J. Chen, S. H. Xu, G. G. Huang, W. H. Chen and L. T. Sun, *Chem. Eur. J.*, 2016, **22**, 7357–7362.
27 Z. S. Hosseini, A. Iraji zad, M. A. Ghiass, S. Fardindoost and S. Hatamie, *J. Mater. Chem. C*,2017, **5**, 8966.
28 N. Sakly, A. H. Said, and H. B. Ouada, *Mat. Sci. Semicond. Process.*, 2014, **27**, 130–139.
29 E. Selishcheva, J. Parisi and J. Kolny-Olesiak, *J. Nanopart. Res.*, 2012, **14**, 711.
30 Y. Yu, X. Guan, X. Li, W. Li, L. Jiang and D. Chen, *J. Alloys Compd.*, 2016, **672**, 265–270.
31 C. Liang, G. Meng, Y. Lei, F. Phillipp and L. Zhang, *Adv. Mater.*, 2010, **13**, 1330–1333.
32 E. Selishcheva, J. Parisi and J. Kolny-Olesiak, *J. Nanopart. Res.*, 2012, **14**, 711.
33 X. Xu, J. Zhuang and X. Wang, *J. Am. Chem. Soc.*, 2008, **130**, 12527–12535.
34 X. Zhou, J. Zhang, T. Jiang, X. Wang and Z. Zhu, *Sens. Actuators A*, 2007, **135**, 209–214.
35 X. Wang, B. Ding, J. Yu, M. Wang and F. Pan, *Nanotechnology*, 2010, **21**, 055502.
36 P. J. Qi, T. Zhang, J. R. Shao, B. Yang, T. Fei and R. Wang, S*ens. Actuators B: Chem.*, 2019, **287**, 93–101.
37 Y. Zhu, J. C Chen, H. M. Li, Y. H. Zhu, and J. Q. Xu, *Sens. Actuators B: Chem.*, 2014, **193**, 320–325.
38 J. Xie, H. Wang, Y. H. Lin, Y. Zhou and Y. P. Wu, *Sens. Actuators B: Chem.*, 2013, **177**, 1083–1088.
39 Z. Yuan, H. Tai, Z. Ye, C. Liu, G. Xie, X. Du and Y. D. Jiang, *Sens. Actuators B: Chem.*, 2016, **234**, 145-154.

